



Article

Cycling Stability of Calcium-Impregnated Vermiculite in Open Reactor Used as a Thermochemical Storage Material

Geraint Sullivan , Chris Griffiths , Eifion Jewell , Justin Searle and Jonathon Elvins

SPECIFIC, College of Engineering, Swansea University, Swansea SA2 8PP, UK; c.m.griffiths@swansea.ac.uk (C.G.); e.jewell@swansea.ac.uk (E.J.); j.r.searle@swansea.ac.uk (J.S.); jonathon.elvins@swansea.ac.uk (J.E.)

* Correspondence: g.l.sullivan@swansea.ac.uk

Abstract: Recent research into thermochemical storage (TCS) materials has highlighted their promising potential for seasonal building heating, through energy capture and release during dehydration and hydration cycling. A common TCS material used throughout this investigation was calcium chloride (CaCl₂)-impregnated vermiculite-based salt in matrix (SIM). This material was assessed for its robustness during charging and discharging cycles to assess its behavior and in terms of energy stability and chemical stability; the results of which showed consistent volumetric energy density and maximum temperature changes over seven cycles. The calcium SIM did, however, show a decline in leachable Ca content, which was presumed to be a result of stabilization within the vermiculite, and chloride concentration showed little change over the course of the study. Real-time visualization using a high-resolution microscope of calcium SIM particles showed a salt phase change and migration of liquid salt into the valleys of the lamella. A novel cobalt chloride (CoCl₂) SIM was used to visualize the hydration path across the particle, through distinct color changes depending on hydration state. The results indicated that the topography of the vermiculite played a significant role in the passive hydration modeling.

Keywords: thermochemical storage; calcium chloride; vermiculite; stability; charge and discharge cycling



Citation: Sullivan, G.; Griffiths, C.; Jewell, E.; Searle, J.; Elvins, J. Cycling Stability of Calcium-Impregnated Vermiculite in Open Reactor Used as a Thermochemical Storage Material. *Energies* **2023**, *16*, 7225. <https://doi.org/10.3390/en16217225>

Received: 21 September 2023

Revised: 13 October 2023

Accepted: 21 October 2023

Published: 24 October 2023

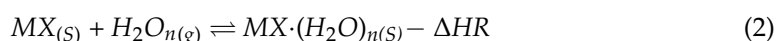
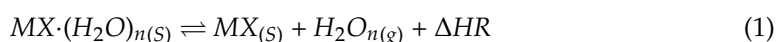


Copyright: © 2023 by the authors. Licensee MDPI, Basel, Switzerland. This article is an open access article distributed under the terms and conditions of the Creative Commons Attribution (CC BY) license (<https://creativecommons.org/licenses/by/4.0/>).

1. Introduction

Global energy prices and greenhouse gas emissions are at an all-time high, with their trend predicted to rise continuously [1–3]. Within the UK, a substantial proportion of energy demand, nearly half (45%), is used for space heating purposes [4] with the majority of this derived from natural gas (exceeding 70%) and other fossil-fuel-derived sources (12%), with a comparatively small proportion derived from renewable resources (<3%) [5,6]. High energy costs have put a huge strain on the cost of living for millions of UK residents, and is imperative to look at alternative, more feasible replacements for space heating. Being a process that captures thermal energy, thermochemical storage (TCS) is thus becoming an attractive alternative method to domestic heating. Unlike sensible heat storage (thermal storage), which uses phase change materials to capture and store heat, such as the melting and solidifying of a wax, TCS captures and releases thermal energy through reversible exotherm/endothrm reactions [7–9], often involving the adsorption and desorption of reactant gas. TCS applications are used to capture solar thermal [10,11] energy or latent heat from an industrial process [10,12,13]. The benefit of using TCS is that it has a high energy density, utilizes inexpensive materials that have a low carbon footprint and is, therefore, potentially a more ‘greener’ and economical choice for domestic heating [9,14,15]. Several parameters need to be considered when selecting TCS storage materials, typically the storage material: must have good thermal conductivity properties for ease of heat transmission, have good cyclability for cost-effectiveness, and have a high energy density [16] for increased energy storage capabilities [17]. To maximize

the stability of TCS materials, often the active ingredients, typically salt hydrates, are incorporated into high surface area materials such as vermiculite, silica gel, or active carbon [18,19], termed salt in matrix (SIM). Studies have shown that salt incorporation improves the cycling stability of the TCS material, showing little to no material hysteresis and enhancing hydration kinetics [16]. To ensure the cost-effectiveness of TCS material, the raw products used in SIM formulations are often cheap, (CaCl₂ (0.2–2 USD/KG) [12] and vermiculite (0.2–44 USD/KG) [18], and its regeneration is conducted at relatively low temperatures <140 °C [19]. In salt hydrate TCM, the energy capture and release occurs from the dehydration and hydration of hygroscopic salts, such as MgSO₄ CaCl₂, Ca(NO₃), Li (NO₃), Li Br, or composite mixtures, [11,20]. During the charging of the material, energy is used to desorb water from hydrated salt crystals, this process is essentially an endothermic reaction and stores thermal energy in the form of ionic bonds [9,16]. To regain that energy, the addition of cooled vapor is adsorbed to the crystal structure, and the formation of coordinate and hydrogen bonds between the crystal structure and water vapor releases heat energy in an exothermic reaction [7,19].



Equations (1) and (2) show the reversible reactions for dehydration and hydration of typical hygroscopic salt (MX). A positive enthalpy change (ΔHR) denotes an endothermic reaction while, conversely, a negative ΔHR states an exothermic reaction.

CaCl₂ incorporated into vermiculite is a particularly good candidate for TCMs and has excellent energy densities (364 kJ/kg, 290 kWh/m³), good moisture uptake, can be regenerated at relatively low temperatures <140 °C, and low toxicity [12,21]. The only issue with CaCl₂ is that deliquescence often occurs from high water adsorption and the hexahydrate has a low melting point around 30 °C [12,21,22]. Impregnating salts within composite materials such as those derived from clays, like vermiculite with CaCl₂, outperformed those of silica, activated carbon, and zeolite, in terms of energy density (305, 123, and 168 kJ/Kg, respectively) [11,23]. Vermiculite is a highly lamellated mineral of magnesium aluminum iron silicate and has a relatively large surface area (15.1 m²/g) and a large pore size of around 3.68 μm in diameter [24], which allows a large amount of salt to be incorporated into the structure, thus maximizing energy density. Vermiculite is ideal as a bulk support material for SIM synthesis as it is a low-cost resource and has been shown to improve hydration pathways and vapor adsorption, and to enhance cycling stability [24]. Aydin et al. (2016) [24], using CaCl₂ vermiculite SIM in an open sorption pipe reactor, achieved an excellent maximum power output of 730 W from 6 Kg of material, with an average temperature output of 24.1 °C over a 20 h period, (highest ΔT of 40 °C at actual humidity 18 g/Kg).

Current research into CaCl₂-impregnated vermiculite SIM has so far focused on optimizing the performance of the material regarding the energy output, moisture uptake, and efficiency of the system used [14,18,21,24–26]. However, there is a lack of information on CaCl₂ behavior proceeding the charging–discharging cycles; in particular, the material’s stability in terms of energy output and its chemical stability [20]. The mode at which humid air interacts with the material is not fully understood, specifically, which areas are more prone to hydration. Visualization techniques used to assess changes of SIM during humidity trials over a small scale will help design larger scale applications in the future to avoid deliquescence and maximize energy output. Cycling stability was achieved using a passive discharger rig to hydrate the SIM in a stream of humid air by removing and then charging using a convection oven. This will be used to investigate in terms of energy output (volumetric density) and maximum temperature difference. CaCl₂ content will be monitored at the end of a complete cycle, by taking a subsample of the SIM and extracting the salt in deionized water. Ion selective electrode analysis will then be used to quantify CaCl₂, providing insights regarding ‘salt loss’ from cycling studies with a possible

correlation of the energy performance data. Additionally, novel microscopy techniques with an adapted flow cell provide visual confirmation regarding the hydration behavior of CaCl_2 in real time. Additionally, a second novel cobalt-impregnated vermiculite (cobalt SIM), was used to visualize hydration pathways on the surface of SIM particles. CoCl_2 goes through several hydration stages, and these changes can be visualized in terms of color changes (anhydrous blue, dihydrate purple, and hexahydrate pink) [27], and it is a good candidate material for hydration modeling.

2. Materials and Method

2.1. Salt in Matrix Preparation

To prepare the salt in matrix (SIM), 100 g of medium-grained vermiculite was purchased from Sinclair™ UK and oven-dried at 120 °C for 2 h to ensure dryness. To the dry vermiculite, a 1:2 ratio by mass of CaCl_2 (purchased from Sigma Aldrich, St. Louis, MI, USA) was added by titration (400 mL) of solution (50 g/100 mL) and allowed to infiltrate via incipient wetness, to form a wet SIM precursor. Repeated mixing during the titration process ensured homogenous uptake of calcium chloride in the generation of the SIM precursor. The SIM precursor was then dried at 120 °C for 24 h to ensure complete drying and generate the charged state; referred throughout as calcium SIM (dry SIM infiltrated with anhydrous calcium chloride).

To prepare the salt in matrix (SIM), for diffusion modeling, 10 g of medium-grained vermiculite was oven-dried at 120 °C for 2 h to ensure dryness. For continuity, a 1:2 ratio by mass of CoCl_2 concentrated solution (40 g/100 mL) (purchased from Sigma Aldrich) was added (50 mL) by incipient wetness to form a wet CoCl_2 SIM precursor. Repeated mixing during the titration process ensured homogenous uptake of CoCl_2 in the generation of the CoCl_2 SIM precursor. The CoCl_2 SIM precursor was then dried at 120 °C for 24 h to generate the blue anhydrous charged state; this will be referred to as cobalt SIM throughout the manuscript. Upon hydration of the anhydrous cobalt SIM (pale blue), several color changes can be observed from the purple dihydrate state to the pink hexahydrate state.

2.2. Thermal Gravimetric Analysis

Thermal gravimetric analysis (TGA) was carried out using a Perkin Elmer TGA1 and differential scanning calorimetry (DSC) was performed on a Perkin Elmer DSC4000. For TGA, 40–50 mg of material was suspended on a platinum sample holder and weight was recorded. The TGA was operated in an oxygen-free environment by using nitrogen as a purge gas at 30 mL per minute. Samples were heated from an initial temperature of 30 °C to 250 °C with a ramp rate of 10 °C per minute.

For DSC, a sample mass between 40 and 50 mg was placed onto an aluminum sample pan and heated in a furnace together with an empty aluminum reference pan. The DSC was operated under the same conditions as the TGA.

2.3. Calcium and Chloride Ion Analysis Using Ion Selective Electrode

An amount of 0.5 g of SIM was added to 50 mL of deionized water, stirred, and left for 1 h, before a 1 mL subsample of the brine was removed and diluted into 50 mL of deionized water.

The diluent of the brine was tested using a multi-ion selective electrode, which can monitor Ca, Cl, K, Na, NO_3 , and Mg ions simultaneously. Prior to analysis, the electrode was conditioned and calibrated, using a low-, medium-, and high-range calibration solution, supplied by clean grow ©.

A blank of the deionized water was tested after calibration, to check whether any carryover was present from the calibration cycle. After analysis of our samples, a calibration check of the medium range was performed to check if there was any drift in the procedure; a tolerance below 15% accuracy was deemed acceptable. LOD of the method was calculated by $3 \times$ standard deviations of 10 replicates of blank samples (deionized water). LOD was determined to be 2.26 mg/L and 0.14 mg/L for calcium and chloride ions, respectively.

2.4. Microscopy

A Keyence VHX-7000 digital microscope was used for time-lapse microscopy to visualize the time-dependent change in surface topography of a SIM particle when subjected to a humid airflow. This microscope uses depth-of-field calculations to ensure that the sample surface topography remains focused throughout the experiment. High-resolution images (3840×2160 pixels) were taken every minute for 30 min at a magnification of $80\times$.

2.5. Humidity Visualisation Analysis

To visualize the discharging procedure, a flow cell was used to mimic conditions experienced in an open-flow reactor. By bubbling nitrogen gas through an impinger containing 250 mL water with a headspace of 250 mL at 2 L per minute, a gas stream with 70% RH (absolute humidity of 12.04 g/m^3) was generated and passed over the SIM particles. Images were captured using depth compositional analysis to give clear textured images.

2.6. Stability Testing

The calcium SIM was cycled by charging and discharging, using an open-top reactor (discharging) and a convection oven (charging) over 7 complete cycles. The reactor comprised a cylindrical vertical vessel, which housed the SIM in a sample basket (diameter 84 mm and height 64 mm), and type K thermocouples ($\pm 2 \text{ }^\circ\text{C}$ accuracy) were placed at the air inlet, within the bulk of the material, and at the output flow. A Cellkraft[®] humidity generator P50 was used to generate a constant flow rate of air at 40 mL per minute with a humidity of 11.2 gM^3 . The discharging of the calcium SIM commenced until the outlet and inlet temperature difference reached $3.5 \text{ }^\circ\text{C}$; this took around 3 h. The discharge SIM was later weighed and placed in the oven overnight to charge the SIM at $120 \text{ }^\circ\text{C}$. This cycle was carried out 7 times, until a suitable trend in data was observed. Below are the energy calculations used in this investigation:

$$\Delta T \text{ }^\circ\text{Cmax} = \text{Max}T^\circ\text{C}(\text{outlet}) - T^\circ\text{C}(\text{inlet}) \quad (3)$$

where $\Delta T \text{ }^\circ\text{Cmax}$ is the greatest change in temperature between the outlet and inlet gas flows.

$$\mu = M * \Delta T * Q(\text{air}) \quad (4)$$

where μ is volumetric density in KwHm^3 ; it is deduced by multiplying the mass of air (M) used by the average temperature change ΔT of the experiment by the specific heat capacity of air Q (air).

$$Q(\text{kJ}) = \frac{\mu/3600}{V(\text{m}^3)} \quad (5)$$

where Q is the energy capacity for the experiment; it converts the μ to kJ per volume (V) of SIM used.

3. Results

3.1. TGA Analysis

Thermal gravimetric analysis was performed on the materials used to synthesize the calcium SIM, to understand the typical mass losses that occur during charging (dehydration) and determine moisture capacity. Separate analysis of the support matrix (dried and non-dried vermiculite) shows very little mass loss, 3.6–5.7%. Therefore, vermiculite does not contribute significantly to mass changes during hydration and dehydration of calcium SIM. Whereas the complete dehydration of pure calcium chloride hexahydrate ($\text{CaCl}_2 \cdot 6\text{H}_2\text{O}$, 218 g/mol) will theoretically lose up to 49.5% of its mass, forming anhydrous CaCl_2 (110 g/mol). To accredit this, TGA and DSC analysis of pure $\text{CaCl}_2 \cdot 6\text{H}_2\text{O}$ showed a comparable mass loss of 49.8%. Each consecutive mass loss is associated with an expulsion of water molecules from the crystal structure. This is clearly seen from the stepwise mass loss on the TGA graph (Figure 1). Complementary to this, the DSC curve illustrates an endothermic change due to energy absorption of vaporization. An endothermic peak

between 30 and 50 °C shows the melting of the hexahydrate. The mass loss of 16.7% between 60 and 131 °C, equates to the loss of 2 moles of water (theoretical mass loss of 16.5%) to form the tetrahydrate associated with a positive DSC endotherm. The next losses between 131 and 180 °C, 200 and 220 °C, and 220 and 240 °C account for the consecutive water losses until the anhydrous salt is formed, where each loss is again associated with a positive endotherm.

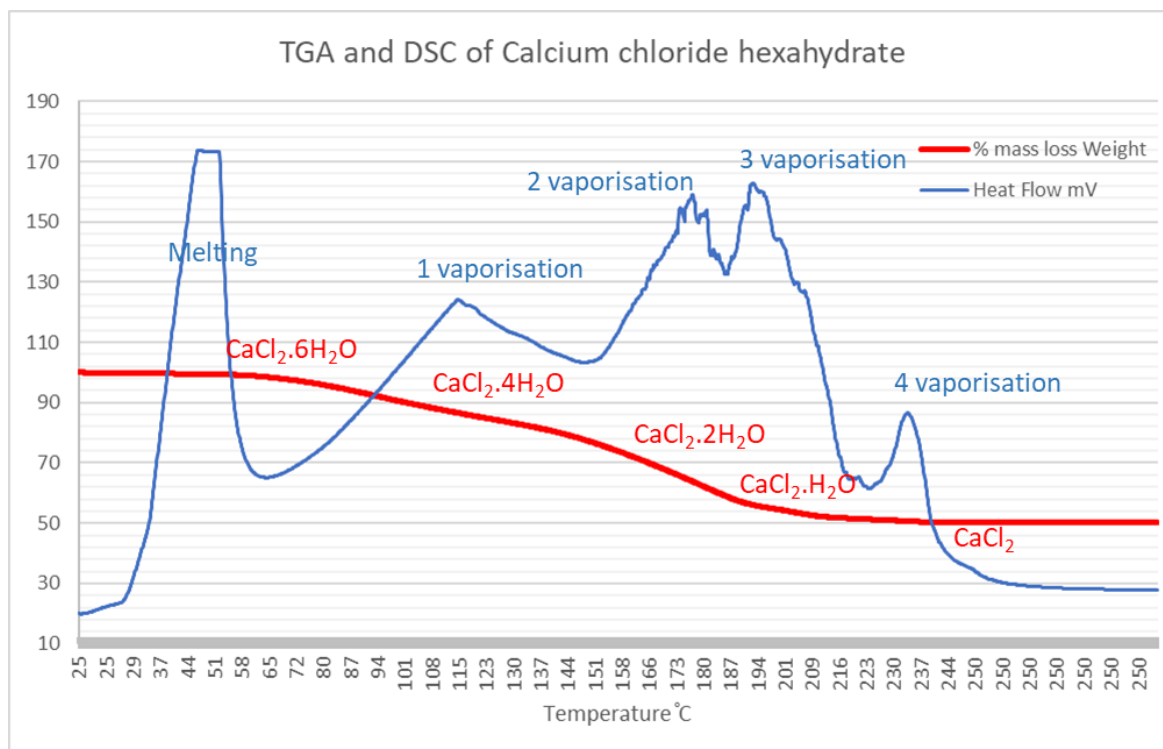


Figure 1. TGA and complementary DSC curves for the dehydration of CaCl₂·H₂O. Each loss equates to the removal of water from the crystal structure.

Using the information gathered previously determining the average CaCl₂ content of the SIM (0.67 g/g) allows us to anticipate the typical moisture uptake of the calcium SIM. For instance, pure anhydrous CaCl₂ will increase by 16.4, 32.7, 65.5, and 98.2% through consecutive hydration steps (mono through to hexahydrate) [22]. As CaCl₂ is approximately 67% of the weight of the impregnated vermiculite, each hydration step can be predicted by a mass increase. Therefore, an adjusted calculation for the different hydration stages of calcium SIM predicts a mass increase of 11.0% for monohydrate, 22.1% for dihydrate, 43.9% for tetrahydrate, and 65.8% for hexahydrate. Although these values are predictors, it is a useful tool to gauge the state of the calcium SIM, as a cut-off limit above 70% would indicate salt deliquescence and an assumed perfect moisture distribution.

An analysis of SIM material using TGA, as shown in Figure 2, demonstrates that the exposure of the material to different conditions affects the overall hydration state of the material. In low-humidity air (30% RSH for 24 h) for longer periods of time, although equating to a substantial mass loss (40%), the majority of the calcium chloride will likely be in a tetra hydrous state, whereas exposure to higher humidity air for a shorter time periods (2 h) equates to a greater mass loss (53%). It is, therefore, likely that more calcium chloride is converted to the hexahydrate state at a higher humidity. This signifies the importance of mass analysis of SIM prior to charging and discharging, in order to determine its potential hydration state, as a means to avoid potential deliquescence.

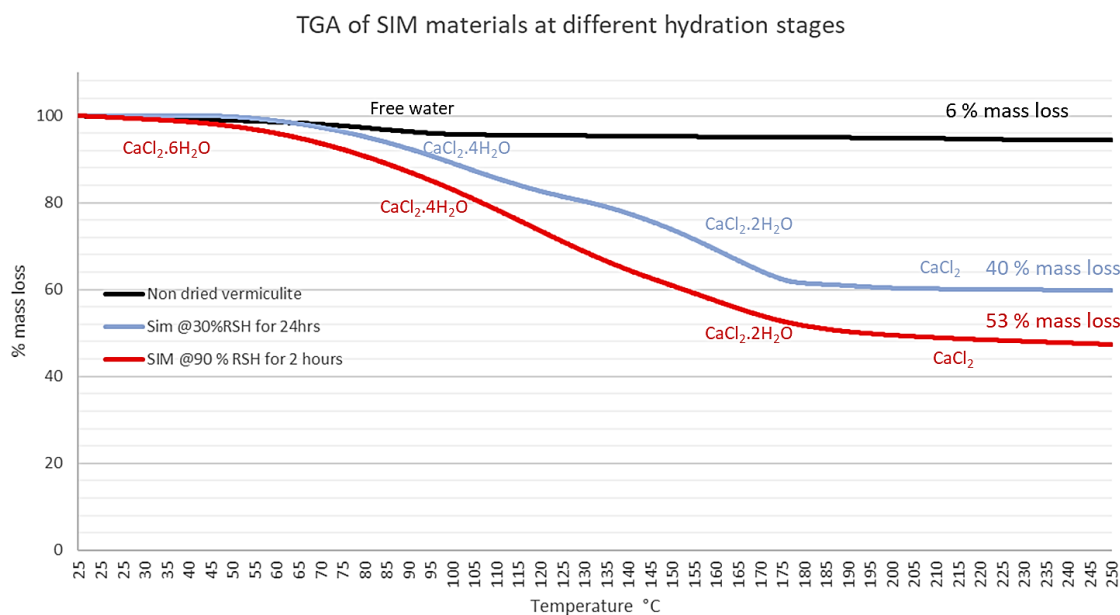


Figure 2. The TGA graphs for the mass losses of A, non-dried virgin vermiculite, and Calcium SIM exposed at two different environments; B, calcium SIM exposed to 90% RSH at 25 °C for 2 h; and C, at 30% RSH at 30 °C for 24 h shows a mass loss of 53% and 40%, respectively.

3.2. Visualization of SIM during Hydration

Monitoring the changes of calcium SIM using a flow cell, connected to moist air flow (12.04 g/m^3) with the Keyence microscope, shows that the calcium vermiculite dramatically changes to the particle during passive hydration. Time lapse was performed over 30 min ($80\times$ magnification) with Images A–D in Figure 3, showing the first 10 min. The hydration of CaCl_2 is very rapid and the surface appears moist after the first minute. The apparent phase change of CaCl_2 on the vermiculite support is surface-driven and is clearly visible by minute five. The liquid salt appears to form a crevasse in the spaces between the lamella and starts to flow; it is possible that hydrated CaCl_2 penetrates deeper into the vermiculite matrix (Figure 4B–D, green arrow). Measurements of the length and breadth of the particles pre- and post-passive hydration show an average loss in size of 3.99%, with some measurements showing up to 9.7% in size reduction. The edges of the lamella protrude, indicating exposure at the edges is preferable.

Due to the translucency of CaCl_2 salt, it is difficult to determine whether hydration is localized to a particular area, occurs instantaneously across the particle, or is diffusion-dependent due to the topography. There is an apparent darkening in color over the duration of the experiment. Color profiling using microscope software (ImageJ version 1.4g) across the particle, which measures, red, green, and blue light intensities, showed a positive increase in red intensity (13%) and a decrease in blue light intensities (20%), indicating darkening across the particle, but difficult to determine.

To get a clearer idea of the mechanism of hydration, a novel cobalt SIM was used to study this potential hydration path; CoCl_2 is another hygroscopic salt, which goes through several hydration states, (anhydrous, dihydrate, and hexahydrate), with a key difference being that the hydration states have an observable color change. In its anhydrous state, CoCl_2 is bright blue; it changes quickly to purple in the in-between dihydrate state, and when fully hydrated, it is a bright pink color.

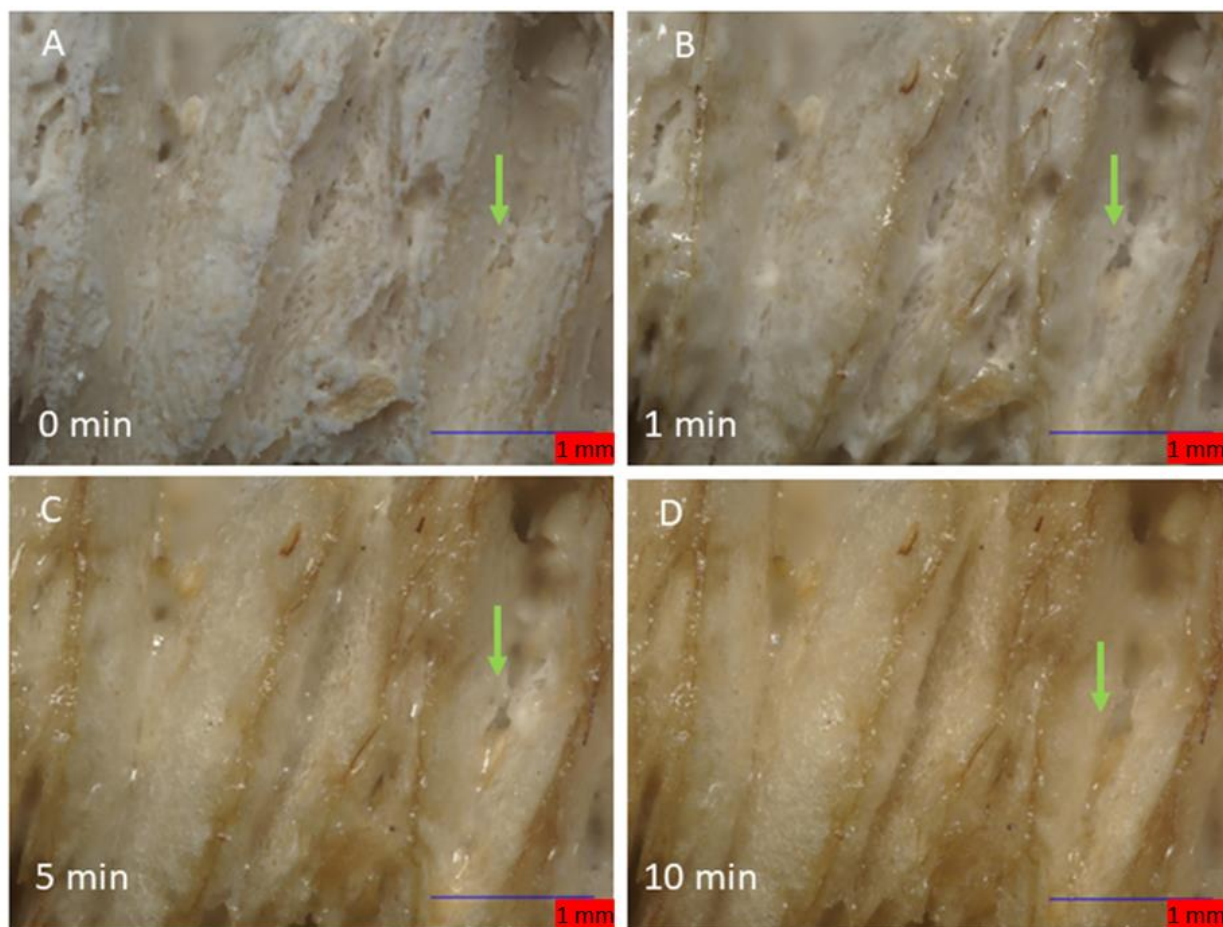


Figure 3. The stages of hydration of a calcium SIM particle: (A) (0 min) shows an anhydrous crystalline structure. Shortly after 1 min (B), the salt becomes ‘wet’ due to rapid hydration. Edges of the vermiculite begin to appear. After 5 and 10 min (C,D), liquid salt appears to melt and migrate down the valleys of the lamella. Green arrow shows a crevasse been formed in between the lamella.

Unlike calcium SIM, the cobalt-impregnated SIM increased in size to around 5.42% during hydration, with some particle thickness expanding up to 14.15%. This is evidence that the crystal structure increases in size during hydration and there is no apparent melting on the surface of the support material. Time-elapse images (80× magnification) of a cobalt SIM particle (Figure 4) show sequential steps in the hydration process. The outer exposed edges of the particle, often closest to the flow, are hydrated first, and a path migrates across the particle, leaving the inter-lamella folds as the last areas to become exposed to water vapor. To visualize this graphically, RGB intensity analysis was performed across particle images at the same location on images at 0, 5, 10, 15, 20, and 30 min to illustrate the progressive change in hydration across the particle. The RGB profiles (Figure 4) correspond with the images in Figure 5 (red arrow). At 0 min, blue light intensity is predominant across the particle being in an anhydrous state as the flow rate is off at this point (gas flow enters right to left of the particle). Time-elapse images show the color remains blue, until around 5 min, whereby edges of the particle start to show areas of pink and purple (see Supplementary Materials), then the color intensifies over the course of the next 5 min, and by 10 min, the tops of the lamella edges are hydrated pink. RGB analysis at 10 min shows red light intensity crossing over to blue light with some overlap in places. Overlap suggests a purple transition and the dihydrate state, whilst a clear cross-over in red color (red arrow Figure 5b) states the formation of the pink hexahydrate. Troughs in the profiles are likely to be the valleys between the lamella; they remain blue until 10 min exposure, suggesting they remain in an anhydrous state. It is not until 15 min (see Supplementary Materials))

of exposure that there are notable areas of transition to dihydrate (purple) in the valleys. By 20 min, RGB profiles still show the deepest trough remaining blue, but most of the shallower troughs have overlapped between red and blue intensity, indicating some of the spaces between the lamella transitioning to a dihydrate state. The exposed edges of the particle are firmly hydrated, with RGB profiles showing complete cross-over to the red light. It is not until the profile at 30 min, which shows the deepest troughs beginning to overlap red and blue intensities, suggesting that deeper penetration of moisture is therefore diffusion-dependent (time-dependent).

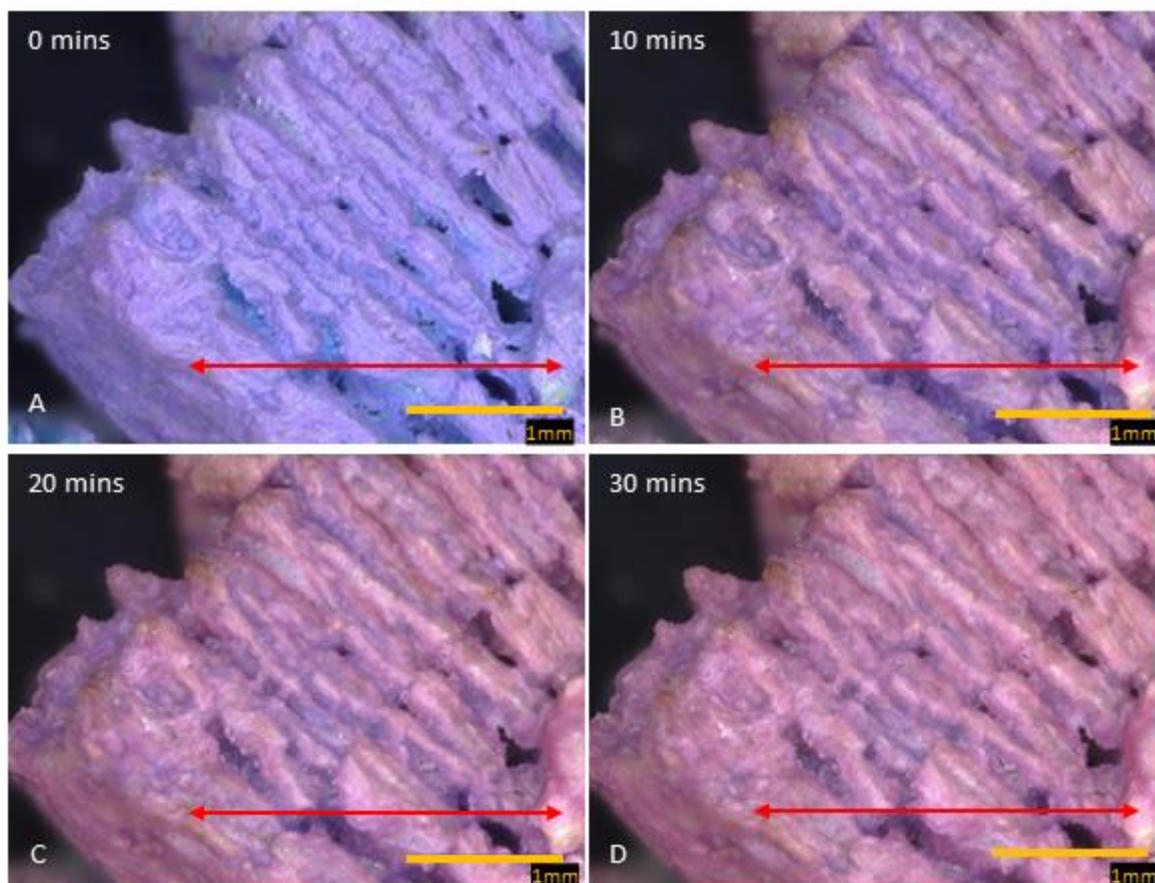


Figure 4. Images of cobalt SIM particle, exposed to moist gas stream, viewed over 30 min. The change in color from blue (A), purple (B,C), to pink (D) signifies various hydration states (anhydrous, dihydrate, and hexahydrate). The inter-lamella spaces take longer to become fully hydrated and even after 30 min, blue/purple color is noticeable. The red arrow across the particle shows where the RGB profile analysis was conducted.

The visualization experiment provides insight into the mechanism of hydration, and it is therefore anticipated that the reaction will proceed quickly, initially at the outer edges of the lamella, which are hydrated first. Salt within the core of the particle will take longer to react with the moisture as the inter-lamella spaces will be hydrated as determined by diffusion. Therefore, it is likely that the complete reaction of calcium chloride in the SIM will span over a longer time, which is beneficial for a heat storage material to have a long temperature profile.

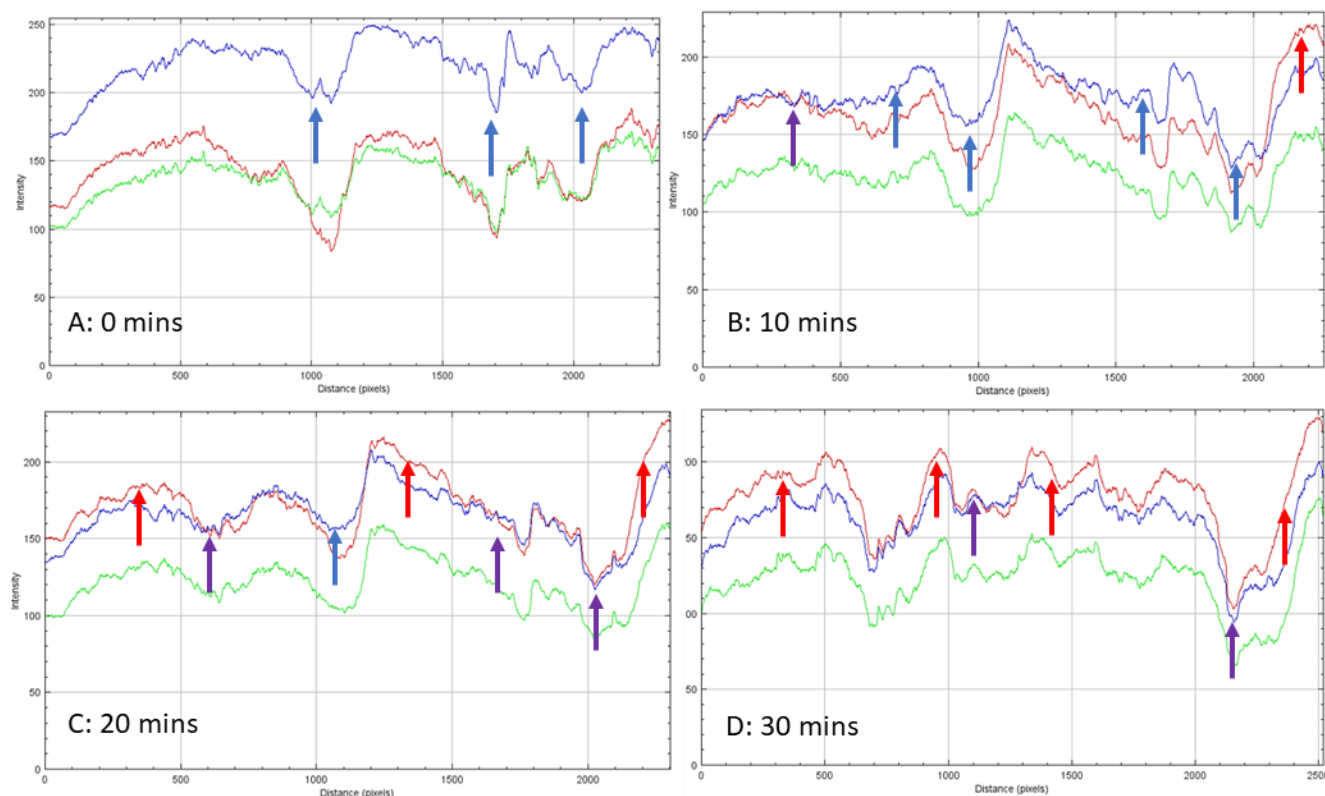


Figure 5. RGB profiles conducted across the cobalt SIM particle shown in Figure 6: (A). Zero minutes shows the particle reflecting predominantly blue light indicating the anhydrous state (blue arrow). Over time overlaps (purple arrow) indicate a possible dihydrate state; these are evident in (B,C) (after 10 and 20 min). A clear cross-over of the red-light (red arrow) intensity signifies the hexahydrate state for CoCl_2 and is apparent in (D) (after 30 min).

3.3. Cycling and Discharge Stability

An initial trial for cycling calcium SIM was performed using our discharge rig mentioned in Section 2.6. Reaction time was carried out until a difference of $3.5\text{ }^\circ\text{C}$ was achieved from the inlet air temperature to the outlet air temperature. A plot of this difference was used to generate a temperature profile for the calcium SIM. The data obtained from the discharge rig were used to calculate the maximum temperature change (ΔT), energy capacity (Q), and volumetric air density (μ), as described in Section 2.6.

After the discharge cycle, the calcium SIM was charged (dried) overnight at $120\text{ }^\circ\text{C}$ in an oven, and a subsample (0.5 g in triplicate) of the material was tested for its chloride and calcium concentration, using the leachate and IEC test described in Section 2.3.

The calcium SIM showed an initial increase in energy output from cycle 1 to cycle 2, with $\Delta T\text{ }^\circ\text{C}$ max increasing from 7.15 to $9.26\text{ }^\circ\text{C}$. However, the initial volumetric density- (μ) of 89.55 kWh/m^3 appears to decrease by cycle 3, to 56.42 kWh/m^3 (Q also follows the same trend); this is a possible result from random packing of the calcium SIM particles, which may result in some restricted airflow throughout the material. The results of the preceding discharge cycles (cycles 4–7) show the increase in energy density (μ) and $\Delta T\text{ }^\circ\text{C}$ max to be that of around 100 kWh/m^3 with highs of ΔT of $11.3\text{ }^\circ\text{C}$. The results show an apparent stabilization in energy data, as seen in Figure 6.

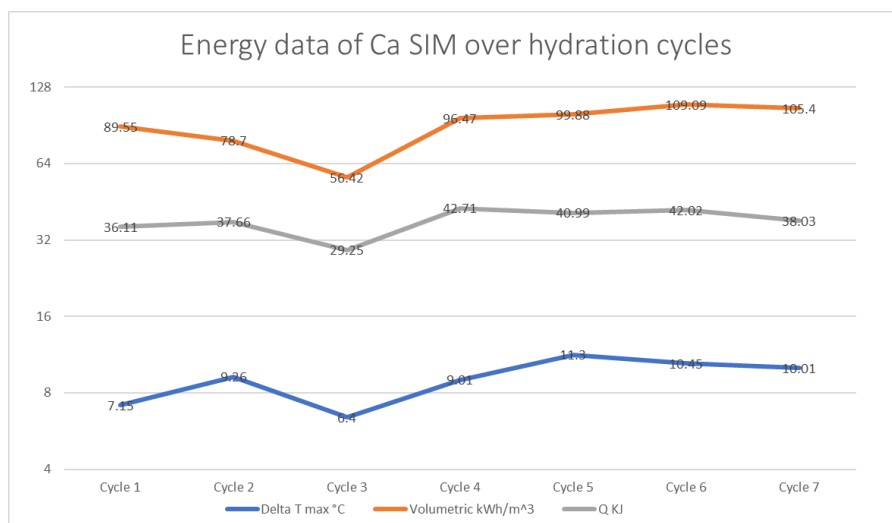


Figure 6. A plot of volumetric energy density (μ), energy capacity (Q), and ΔT max °C of calcium SIM that has undergone discharge and charge cycling studies.

A comparison of the calcium and chloride ion content of the calcium SIM running alongside the cycling stability shows that calcium ion distribution in the leachate tends to decrease over the charging cycle. The results for calcium ion release in cycles 2–7 show a statistical difference when compared to the initial concentration (RSD < 15% for repeat analysis). However, the same is not seen for the counter ion (chloride), as levels show no statistical change and are at a consistent level (RSD < 15% for repeat analysis) over the course of the trial (Figure 7). It is postulated that the calcium ions are not lost from the material, as a decrease in chloride content would also be apparent, but calcium may in fact stabilize within the vermiculite structure over successive cycles, by binding or chelating to the structure, making it less likely to leach out [28–32]. Whereby the chloride ions remain free to dissolve and are less tightly bound. This stabilization effect of calcium may account for the stabilization effect seen in the energy data in Figure 6 (ΔT , Q, and μ)

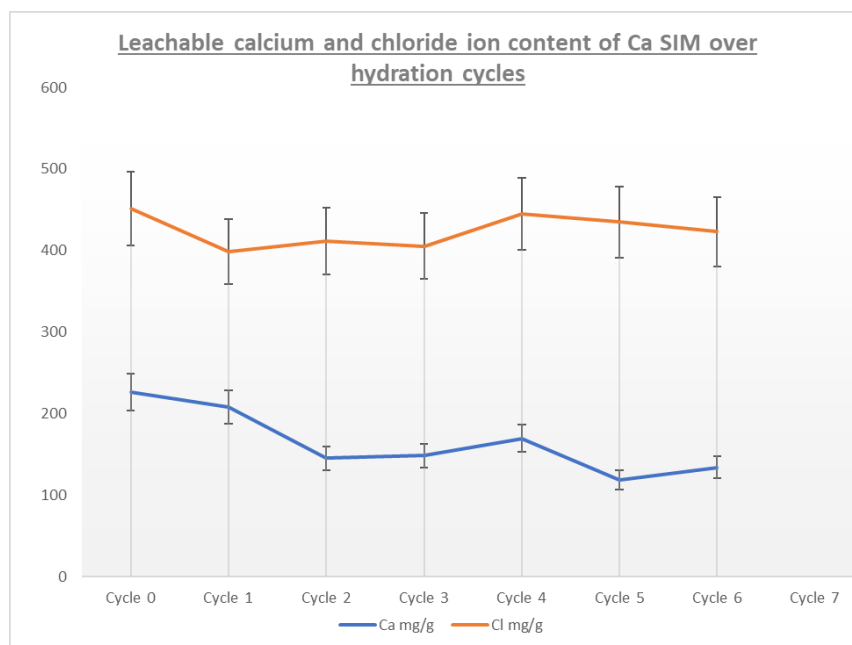


Figure 7. A plot of leachable Ca and Cl ions taken after discharge and charge cycles, in order to understand ion losses or migration.

4. Conclusions

Material performance testing is the main driving force for the selection of thermal chemical storage materials (i.e., energy output and efficiency). However, fundamental characterizations, such as cycling stability, salt content assessment, and material modeling, are equally important to determine the viability of a product in terms of its reuse and predictors of its energy release profile. The results from this study show promising cycling potential for CaCl₂ SIM; this small-scale cycling study shows an improvement in energy output over the course of the study, which appears to stabilize by day 7, highlighting its potential for repeated use in terms of heat storage and release [20]. This stabilization was evidenced by the apparent retainment of calcium ions within the vermiculite matrix. However, there are concerns over successive cycles in the mechanical strength of the vermiculite, as it is predicted that the structure will likely fail over larger cycles as was seen in other studies [16,20]. Modeling the moisture uptake of the SIM provided important information that will help develop future materials for thermal chemical storage, and refine the technology used to house the seasonal storage material to ensure optimal particle hydration and energy output.

This research highlights that fundamental characterization would assist in the selection of a material; a material with good salt uptake and mechanical and chemical stability will produce a more sustainable and energy-efficient product in the long term.

Supplementary Materials: The following supporting information can be downloaded at: <https://www.mdpi.com/article/10.3390/en16217225/s1>, Figure S1: Table of chlorine and calcium concentration, Figure S2: Energy profile data for cycling study, Figure S3, Sequential images of hydration of Calcium SIM, Figure S4 images of cobalt SIM hydration in passive flow cell, Figure S5 additional images of Cobalt SIM during hydration with respective RGB profiles.

Author Contributions: Conceptualization, G.S.; Methodology, G.S.; Formal analysis, G.S.; Investigation, C.G.; Writing—original draft, G.S.; Writing—review & editing, E.J. and J.S.; Supervision, J.E. All authors have read and agreed to the published version of the manuscript.

Funding: This research was funded by FLEXIS project (reference 80835), and was part-funded by the European Regional Development Fund (ERDF) through the Welsh Government. This financial support is gratefully acknowledged.

Acknowledgments: We would also like to thank Gareth Davies and Kate Johns of Tata Steel Europe Group for ICP-MS and IEC analysis and acknowledge the support from Anthony Lewis of Specific for the construction of the flow cell used in passive humidity testing.

Conflicts of Interest: This article is the result of authors own investigation, except where otherwise stated. Other sources are acknowledged by explicit references. The author confirms that the material has not been published previously in whole or part, or abstract form and does not conflict interest with any other third parties.

References

1. International Energy Agency. Review 2021 Assessing the Effects of Economic Recoveries on Global Energy Demand and CO₂ Emissions in 2021 Global Energy. Available online: www.iea.org/t&e/ (accessed on 9 October 2023).
2. International Energy Agency. Global Energy Review: CO₂ Emissions in 2021 Global Emissions Rebound Sharply to Highest Ever Level. 2021. Available online: <https://www.iea.org/reports/global-energy-review-co2-emissions-in-2021-2> (accessed on 11 October 2023).
3. Institute for Government. Cost of Living Crisis. 2022. Available online: <https://www.instituteforgovernment.org.uk/explainer/cost-living-crisis> (accessed on 11 October 2023).
4. Mitchell, R.; Natarajan, S. UK Passivhaus and the Energy Performance Gap. *Energy Build.* **2020**, *224*, 110240. [CrossRef]
5. Energy Tutorial: Energy and Sustainability What's Energy Used for? Available online: <https://www.gov.uk/government/collections/energy-consumption-in-the-uk> (accessed on 9 October 2023).
6. Gielen, D.; Boshell, F.; Saygin, D.; Bazilian, M.D.; Wagner, N.; Gorini, R. The Role of Renewable Energy in the Global Energy Transformation. *Energy Strategy Rev.* **2019**, *24*, 38–50. [CrossRef]
7. Aydin, D.; Casey, S.P.; Riffat, S. The Latest Advancements on Thermochemical Heat Storage Systems. *Renew. Sustain. Energy Rev.* **2015**, *41*, 356–367. [CrossRef]

8. Trausel, F.; de Jong, A.J.; Cuypers, R. A Review on the Properties of Salt Hydrates for Thermochemical Storage. *Energy Procedia* **2014**, *48*, 447–452. [[CrossRef](#)]
9. Donkers, P.A.J.; Sögütoglu, L.C.; Huinink, H.P.; Fischer, H.R.; Adan, O.C.G. A Review of Salt Hydrates for Seasonal Heat Storage in Domestic Applications. *Appl. Energy* **2017**, *199*, 45–68. [[CrossRef](#)]
10. Zhang, Y.; Chen, Z.; Kutlu, C.; Su, Y.; Riffat, S. Investigation on a Vermiculite-Based Solar Thermochemical Heat Storage System for Building Applications. *Future Cities Environ.* **2022**, *8*, 1–14. [[CrossRef](#)]
11. Jarimi, H.; Devrim, A.; Zhang, Y.; Ding, Y.; Ramadan, O.; Chen, X.; Dodo, A.; Utlu, Z.; Riffat, S. Materials Characterization of Innovative Composite Materials for Solar-Driven Thermochemical Heat Storage (THS) Suitable for Building Application. *Int. J. Low-Carbon Technol.* **2018**, *13*, 30–42. [[CrossRef](#)]
12. N'Tsoukpoe, K.E.; Rammelberg, H.U.; Lele, A.F.; Korhammer, K.; Watts, B.A.; Schmidt, T.; Ruck, W.K.L. A Review on the Use of Calcium Chloride in Applied Thermal Engineering. *Appl. Therm. Eng.* **2015**, *75*, 513–531. [[CrossRef](#)]
13. Manente, G.; Ding, Y.; Sciacovelli, A. A Structured Procedure for the Selection of Thermal Energy Storage Options for Utilization and Conversion of Industrial Waste Heat. *J. Energy Storage* **2022**, *51*, 104411. [[CrossRef](#)]
14. Ait Ousaleh, H.; Sair, S.; Zaki, A.; Faik, A.; Mirena Igartua, J.; el Bouari, A. Double Hydrates Salt as Sustainable Thermochemical Energy Storage Materials: Evaluation of Dehydration Behavior and Structural Phase Transition Reversibility. *Sol. Energy* **2020**, *201*, 846–856. [[CrossRef](#)]
15. Tetteh, S.; Yazdani, M.R.; Santasalo-Aarnio, A. Cost-Effective Electro-Thermal Energy Storage to Balance Small Scale Renewable Energy Systems. *J. Energy Storage* **2021**, *41*, 102829. [[CrossRef](#)]
16. Aarts, J.; van Ravensteijn, B.; Fischer, H.; Adan, O.; Huinink, H. Polymeric Stabilization of Salt Hydrates for Thermochemical Energy Storage. *Appl. Energy* **2023**, *341*, 121068. [[CrossRef](#)]
17. Bird, J.E.; Humphries, T.D.; Paskevicius, M.; Poupin, L.; Buckley, C.E. Thermal Properties of Thermochemical Heat Storage Materials. *Phys. Chem. Chem. Phys.* **2020**, *22*, 4617–4625. [[CrossRef](#)] [[PubMed](#)]
18. Ramadan, O.; Zhang, Y.; Ding, Y.; Jarimi, H.; Dodo, A.; Riffat, S. Synthesis and Characterization of Salt in Matrix Composite Materials for Open Cycle Thermochemical Heat Storage for Building Applications. 2017. Available online: <https://www.researchgate.net/publication/326190703> (accessed on 11 October 2023).
19. Mohapatra, D.; Nandanavanam, J. Salt in Matrix for Thermochemical Energy Storage—A Review. *Mater. Today Proc.* **2023**, *72*, 27–33. [[CrossRef](#)]
20. Chen, Z.; Zhang, Y.; Zhang, Y.; Su, Y.; Riffat, S. A Study on Vermiculite-Based Salt Mixture Composite Materials for Low-Grade Thermochemical Adsorption Heat Storage. *Energy* **2023**, *278*, 127986. [[CrossRef](#)]
21. Xie, N.; Huang, Z.; Luo, Z.; Gao, X.; Fang, Y.; Zhang, Z. Inorganic Salt Hydrate for Thermal Energy Storage. *Appl. Sci.* **2017**, *7*, 1317. [[CrossRef](#)]
22. Vainio, E.; Demartini, N.; Hupa, L.; Åmand, L.E.; Richards, T.; Hupa, M. Hygroscopic Properties of Calcium Chloride and Its Role on Cold-End Corrosion in Biomass Combustion. *Energy Fuels* **2019**, *33*, 11913–11922. [[CrossRef](#)]
23. Casey, S.P.; Elvins, J.; Riffat, S.; Robinson, A. Salt Impregnated Desiccant Matrices for “open” Thermochemical Energy Storage—Selection, Synthesis and Characterisation of Candidate Materials. *Energy Build.* **2014**, *84*, 412–425. [[CrossRef](#)]
24. Aydin, D.; Casey, S.P.; Chen, X.; Riffat, S. Novel “Open-Sorption Pipe” Reactor for Solar Thermal Energy Storage. *Energy Convers. Manag.* **2016**, *121*, 321–334. [[CrossRef](#)]
25. Gordeeva, L.G.; Aristov, Y.I. Composites “salt inside Porous Matrix” for Adsorption Heat Transformation: A Current State-of-the-Art and New Trends. *Int. J. Low-Carbon Technol.* **2012**, *7*, 288–302. [[CrossRef](#)]
26. Walsh, S.; Reynolds, J.; Abbas, B.; Woods, R.; Searle, J.; Jewell, E.; Elvins, J. Assessing the Dynamic Performance of Thermochemical Storage Materials. *Energies* **2020**, *13*, 2202. [[CrossRef](#)]
27. Schramm, C.; Kitzke, A.; Tessadri, R. Cobalt Chloride-Based Humidity Sensor Attached to SOL-GEL Modified Cellulosic Material. *Cellul. Chem. Technol.* **2017**, *51*, 273–282.
28. Ferreira, D.R.; Thornhill, J.A.; Roderick, E.I.N.; Li, Y. The Impact of PH and Ion Exchange on 133 Cs Adsorption on Vermiculite. *J. Environ. Qual.* **2018**, *47*, 1365–1370. [[CrossRef](#)] [[PubMed](#)]
29. Huang, K.; Rowe, P.; Chi, C.; Sreepal, V.; Bohn, T.; Zhou, K.G.; Su, Y.; Prestat, E.; Pillai, P.B.; Cherian, C.T.; et al. Cation-Controlled Wetting Properties of Vermiculite Membranes and Its Promise for Fouling Resistant Oil–Water Separation. *Nat. Commun.* **2020**, *11*, 1097. [[CrossRef](#)]
30. Hailu, Y.; Tilahun, E.; Brhane, A.; Resky, H.; Sahu, O. Ion Exchanges Process for Calcium, Magnesium and Total Hardness from Ground Water with Natural Zeolite. *Groundw. Sustain. Dev.* **2019**, *8*, 457–467. [[CrossRef](#)]
31. Levy, R.; Shainberg, I. *Calcium-Magnesium Exchange in Montmorillonite and Vermiculite*; Pergamon Press: Oxford, UK, 1972; Volume 20. Available online: <https://www.researchgate.net/publication/237661151> (accessed on 11 October 2023).
32. Feng, J.; Liu, M.; Fu, L.; Zhang, K.; Xie, Z.; Shi, D.; Ma, X. Enhancement and Mechanism of Vermiculite Thermal Expansion Modified by Sodium Ions. *RSC Adv.* **2020**, *10*, 7635–7642. [[CrossRef](#)] [[PubMed](#)]

Disclaimer/Publisher’s Note: The statements, opinions and data contained in all publications are solely those of the individual author(s) and contributor(s) and not of MDPI and/or the editor(s). MDPI and/or the editor(s) disclaim responsibility for any injury to people or property resulting from any ideas, methods, instructions or products referred to in the content.